Chemistry & Biology, Vol. 11, 565–573, April, 2004, ©2004 Elsevier Science Ltd. All rights reserved. DOI 10.1016/j.chembiol.2004.03.017

A Bacterial Acetyltransferase Capable of Regioselective *N*-Acetylation of Antibiotics and Histones

Matthew W. Vetting, Sophie Magnet, Edward Nieves, Steven L. Roderick, and John S. Blanchard*
Department of Biochemistry
Albert Einstein College of Medicine
1300 Morris Park Avenue
Bronx, New York 10461

Summary

The *Salmonella enterica* chromosomally encoded AAC(6′)-Iy has been shown to confer broad aminoglycoside resistance in strains in which the structural gene is expressed. The three-dimensional structures reported place the enzyme in the large Gcn5-related *N*-acetyltransferase (GNAT) superfamily. The structure of the CoA-ribostamycin ternary complex allows us to propose a chemical mechanism for the reaction, and comparison with the *Mycobacterium tuberculosis* AAC(2′)-CoA-ribostamycin complex allows us to define how regioselectivity of acetylation is acheived. The AAC(6′)-Iy dimer is most structurally similar to the *Saccharomyces cerevisiae* Hpa2-encoded histone acetyltransferase. We demonstrate that AAC(6′)-Iy catalyzes both acetyl-CoA-dependent self-α-*N*-acetylation and acetylation of eukaryotic histone proteins and the human histone H3 N-terminal peptide. These structural and catalytic similarities lead us to propose that chromosomally encoded bacterial acetyltransferases, including those functionally identified as aminoglycoside acetyltransferases, are the evolutionary progenitors of the eukaryotic histone acetyltransferases.

Introduction

Aminoglycosides were one of the first natural products identified as antibacterial agents and bind to the acceptor site (A site) of the 30S ribosomal subunit, where they inhibit protein synthesis by inhibiting initiation and cause code misreading [1]. Resistance to aminoglycosides is of increasing clinical concern and may be due to target modification, including rRNA methylation in aminoglycoside-producing organisms [1] or mutations in the 16S rRNA or the S12 protein in *M. tuberculosis* [2]. However, the vast majority of clinical resistance to aminoglycosides results from the expression of enzymes that covalently modify the drug [3]. These include enzymes that catalyze either ATP-dependent *O*-phosphorylation or *O*-adenylylation and those that catalyze the acetyl-CoA-dependent *N*-acetylation of the drug. The plasmid-encoded *N*-acetyltransferases can act on essentially all clinically useful aminoglycosides and are responsible for the majority of worldwide clinical resistance to aminoglycosides in Gram-negative pathogenic bacteria. A number of different regioisozymes have been identified, but those that acetylate either the 6′- or 3-amino substituents are the most prevalent in aminoglycoside-resistant clinical strains [4].

A chromosomally encoded aminoglycoside 6′-*N*-acetyltransferase has been identified in a clinical strain of aminoglycoside-resistant *S. enterica* [5]. This normally cryptically expressed gene was implicated in the resistant phenotype as a result of a massive 60 Kbp genomic deletion that placed the constitutive promoter of the *nmpC*-encoded outer membrane porin directly upstream of the *sgcE, -R*, and *aac(6′)* genes, resulting in the constitutive expression of the *aac(6′)-Iy* gene (Figure 1A). The predicted 145 amino acid enzyme showed significant primary sequence homology with other aminoglycoside 6′-acetyltransferases and members of the Gcn5-related *N*-acetyltransferase (GNAT) superfamily. The *aac(6′)-Iy* gene was expressed and the purified protein was shown to catalyze the regioselective 6′-*N*-acetylation of a broad array of aminoglycosides, including ribostamycin (Figure 1B) [6]. The enzyme binds aminoglycoside substrates and acetyl-CoA randomly and synergistically, with the release of the product CoA being rate limiting [7].

Results and Discussion

Structure Determination

Diffraction data at three X-ray wavelengths of the Se-Met-substituted *S. enterica* AAC(6′)-Iy were used to solve the structure by multiwavelength anomalous diffraction (Table 1). The tertiary structure of the *S. enterica* AAC(6′)-Iy monomer (Figure 2A) is similar to those observed previously for aminoglycoside acetyltransferases and other members of the GCN5-related *N*-acetyltransferase (GNAT) superfamily [8, 9]. The N-terminal region is composed of a short β strand (β1) and two α helices (α1 and α2, all shown in green in Figure 2A). The completely conserved secondary structural elements of this fold are the three antiparallel strands (β2–4, shown in yellow), the long, central helix and adjacent strand (α3 and β5, shown in red) and the carboxy-terminal α helix (α4, shown in blue). The pantetheine arm of coenzyme A binds between β4 and β5 in a manner similar to all other GNAT members [10]. The assembly of the catalytically active dimer generates a continuous β sheet that includes β1–6 from one monomer and β6′–1′ of the adjacent monomer (Figure 2B). However, β6 of one monomer is domain swapped between β5′ and β6′ of the adjacent monomer. Although not added in the crystallization solutions, clear electron density due to bound CoA was observed in both subunits.

Intimate contacts between adjacent dimers in the two different native crystal forms (Table 1) involve the N-terminal His_6/thrombin cleavage extension of one dimer with an adjacent dimer (Figure 2C). The electron density observed in both native crystal forms allows for the unambiguous identification and positioning of the

*Correspondence: blanchar@aecom.yu.edu

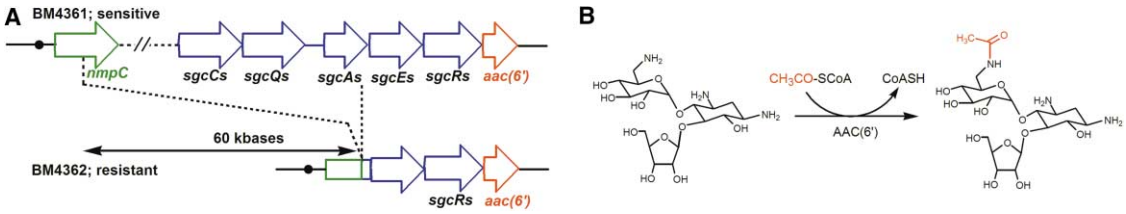

Figure 1. Schematic of the Genomic Environment and a Typical Acetyltransferase Reaction of AAC(6′)-Iy

(A) The genomic environment of the aminoglycoside-sensitive *S. enterica* BM4361 and aminoglycoside-resistant *S. enterica* BM4362. A 60 kilobase pair chromosomal deletion results in the constitutive *nmpC* promoter (black circle) being placed ~2.2 kilobases upstream of the *aac(6′)-Iy*-encoded aminoglycoside acetyltransferase (red arrow).

(B) Ribostamycin acetylation catalyzed by aminoglycoside 6′-N-acetyltransferase.

peptide in the channel. In both crystal forms, these contacts involve amino acids that are elements of the thrombin cleavage sequence (VPR↓GSH). The peptide is bound in a long surface channel at the dimer interface and is adjacent to the sulfur atom of bound CoA. In Native 2 crystals, the arginine residue of the peptide makes specific, electrostatic contacts with the carboxylate groups of Glu79 and Asp115, and the peptide is bounded top and bottom by the aromatic rings of Trp22 and Tyr66′, respectively (Figure 2D). In Native 1 crystals, the polarity of the peptide orientation is reversed (data not shown).

The structure of the enzyme-CoA-ribostamycin complex was determined by cocrystallizing the enzyme with ribostamycin (Table 1). The quality of the electron density omit map (Figure 3A) allowed for the unambiguous positioning of ribostamycin in the previously described channel (Figure 3B) at the dimer interface and allowed us to identify the binding interactions between the enzyme and this substrate. The 6′-amine is positioned 3.4 Å away from the sulfur atom of bound CoA, a position consistent with both the known regioselectivity and the required chemistry for acetyltransfer from acetyl-CoA. The *S. enterica* acetyltransferase studied here catalyzes the regioselective 6′-N-acetylation of a wide variety of both 4,6- and 4,5-disubstituted deoxystreptamines (e.g., tobramycin, ribostamycin, etc.) [6]. The structure of the CoA-ribostamycin complex clearly indicates that the primed and central rings make extensive electrostatic and hydrogen bonding interactions with the enzyme, while a single interaction is observed between the ribose ring and the imidazole side chain of His25 (Figure 3C). As we observed in the peptide-bound complex, the aromatic rings of Trp22 and Tyr66′ stack above and below the bound aminoglycoside, allowing for little conformational mobility when the substrate is bound (Figure 3D). The amino and hydroxyl groups of the primed and central deoxystreptamine rings make direct contacts with the carboxyl-containing side chains of Glu79, Asp115, and Glu136′ that contribute to the intensely negatively charged active site/dimer interface (Figure 3E). There is sufficient room within the channel to accommodate a sugar ring at the 6 position, arguing that aminoglycoside substrates for the enzyme such as tobramycin and kanamycin would bind in a similar fashion. In addition, the loops connecting α1 and α2 and β3′ and β4′, which

Table 1. Crystallographic Data, Phasing and Refinement Statistics

Data Collection and Phasing

Data Set	Native 1			Peak		
X-Ray Source	Home Source	Native 2	Ribostamycin	BNL X-9X	Inflection	Remote
Wavelength (Å)		CuKα		0.97917	0.97932	0.97152
Resolution (Å)	20–2.4	20–3.0	20–2.0	20–3.2		
Space group	$P3_121$	$P3_221$	C2	$P3_221$		
Unit cell (Å)	$a = 62.8$	$a = 84.5$	$a = 85.0$ $b = 44.7$		$a = 85.1$	
	$c = 157.4$	$c = 66.7$	$c = 88.0$ $\beta = 93.9$		$c = 66.7$	
Completeness (%)	98.0 (95.5)	95.3 (87.0)	93.0 (67.6)	97.9 (94.2)	97.1 (91.4)	89.6 (72.1)
Redundancy	5.0 (4.0)	4.0 (3.0)	3.7 (2.8)	8.9 (5.6)	6.6 (3.7)	2.8 (2.0)
I/sigI (σ)	22.8 (11.7)	19.8 (5.1)	20.8 (10.6)	17.5 (4.8)	13.9 (2.9)	15.6 (3.9)
Rsym (%)	4.6 (9.0)	4.6 (13.6)	3.7 (10.6)	5.9 (16.4)	6.6 (19.4)	5.3 (15.2)

Refinement Statistics

Data Set	Native 1	Native 2	Ribostamycin
R_{cryst} (%)	18.2 (16.8)	22.5 (28.1)	16.7 (17.8)
R_{free} (%)	24.5 (24.5)	26.7 (35.5)	21.0 (22.7)
No. atoms protein/water/other	2270/161/106	1200/–/53	2318/217/169
Average B (Å^2) protein/water/other	26.1/29.2/26.1	57.8/–/62.2	21.3/30.1/24.9
Rmsd bond length (Å)	0.021	0.015	0.021
Rmsd bond angle (°)	2.017	1.950	1.975

Values in parentheses correspond to the data in the highest resolution shell of data.

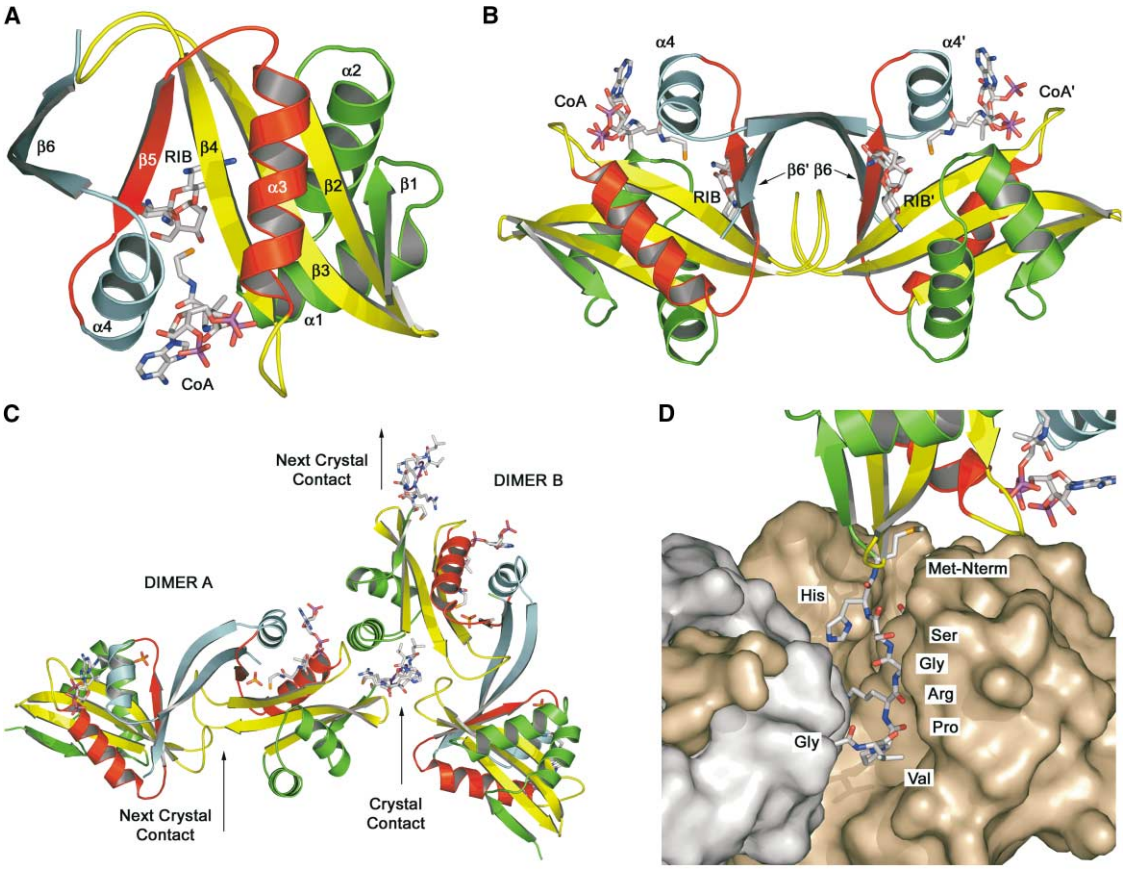

Figure 2. Overall Fold of AAC(6′)-Iy

(A) The crystallographically determined structure of the *S. enterica* AAC(6′)-Iy monomer. The coloring conforms to the amino-terminal residues (β1, α1, α2, green), the central β strands (β2–4, yellow), the central α helix and β strand (α3, β5, red), and the carboxy-terminal region (α4, β6, blue). CoenzymeA and ribostamycin are colored by atom type. This coloring scheme is used throughout.

(B) The *S. enterica* AAC(6′)-Iy dimer showing the position of bound CoA and ribostamycin (stick representation, colored by atom type). The exchange of the β6 and β6′ strands is noted.

(C) The interaction between two *S. enterica* AAC(6′)-Iy dimers showing the N terminally extended peptide, colored by atom type, interacting with an adjacent dimer.

(D) Closeup of the interaction between the crystallographically observable N terminally extended peptide and the active site channel. The dimer is presented in surface representation with each monomer colored in silver or bronze.

contain Trp22 and Tyr66′, respectively, are flexible, allowing variously substituted aminoglycosides to be bound and acetylated. These observations account for the broad substrate specificity of the enzyme for both 4,5- and 4,6-disubstituted deoxystreptamines used clinically.

Chemical Mechanism and Regioselectivity

The acetylation of aminoglycosides occurs after the random binding of both acetyl-CoA and 6′-amine-containing aminoglycosides to the enzyme and has been proposed to proceed via a direct nucleophilic attack by the amine on the thioester [6]. The pantetheine arm of CoA interacts with main chain residues of β4 that include the structurally conserved β bulge, centered at residue E79, on β4. In the structures of acetyl-CoA complexes of other GNAT superfamily members, the carbonyl oxygen of acetylCoA makes a single hydrogen bonding interaction with a backbone amide nitrogen, corresponding to $I81^N$ in our structure [10]. The 6′-amine of ribostamycin is hydrogen bonded to a water molecule and the backbone carbonyl of D115 in the adjacent β5 (Figure 4A), and therefore does not directly interact with a side chain group that could act as a general base. However, this water molecule is, in turn, hydrogen bonded to the carboxyl side chain of D115, where two unusually short hydrogen bonds (<2.65 Å) are observed between (1) the D115 carboxylate and the water molecule and (2) the water molecule and the 6′-amine, suggesting that deprotonation of the amine may occur via this intervening water molecule during the nucleophilic attack on the thioester. There is no obvious candidate for a general acid that could protonate the thiolate anion after collapse of the tetrahedral intermediate. There is a tightly bound sulfate anion at the position where we show a water molecule, and we suggest that thiolate protonation occurs using a water molecule accessible to bulk solvent. The very favorable energetics of the acetyltransfer chemistry and the close proximity of the two reactants apparently are sufficient to promote the chem-

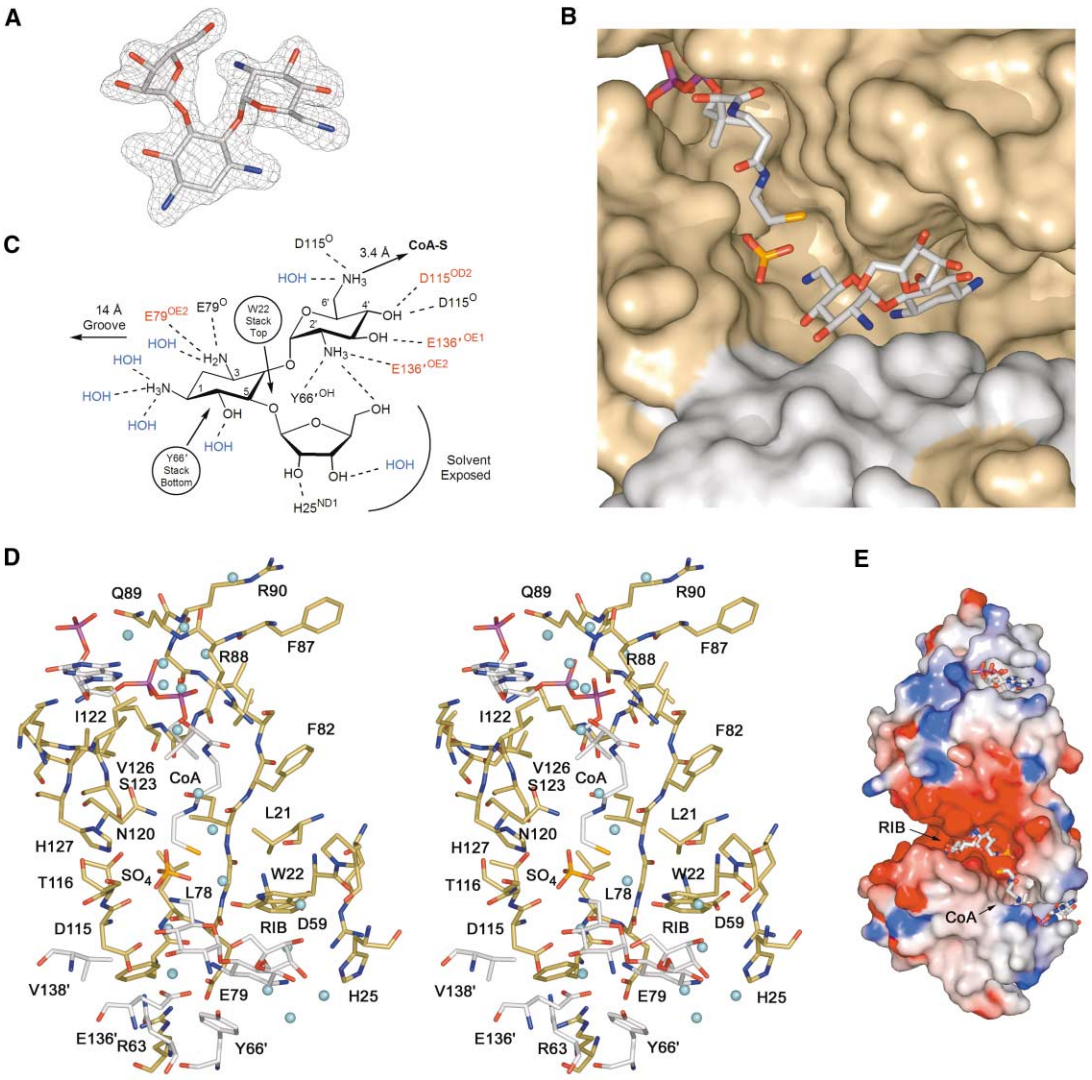

Figure 3. The AAC(6′)-Iy Ribostamycin Complex

(A) Ribostamycin is shown modeled into a F_o-F_c simulated annealing omit electron density map contoured at 3 σ.

(B) Ribostamycin bound at the active site of AAC(6′)-Iy. Both CoA and ribostamycin are colored according to atom type, and each monomer surface is colored in either silver or bronze.

(C) Scheme showing the interactions observed between AAC(6′)-Iy and ribostamycin. Primed residues are contributed by the adjacent monomer.

(D) Stereo diagram of residues in the AAC(6′)-Iy active site that are 5 Å or less from either the CoA or ribostamycin. The coloring of the carbon atoms of each monomer is similar to (B), as is the relative orientation.

(E) A molecular surface of the AAC(6′)-Iy dimer-CoA-ribostamycin complex colored by its electrostatic potential (red, −10 Kt; blue, +10 Kt) as calculated in GRASP [28]. CoA and ribostamycin are represented in stick fashion and colored by atom type, and the peptide/aminoglycoside binding channel is overwhelmingly electronegative.

ical reaction, without the requirement for directly hydrogen-bonded general acid or base groups.

The high-resolution structures of two aminoglycoside acetyltransferase-CoA-ribostamycin complexes (*M. tuberculosis* AAC(2′) [11] and the *S. enterica* AAC(6′)-Iy) permit an examination of how two structurally similar GNATs can bind the same substrates but regioselectively acetylate two amine functions of the same ring. Prior to these studies, multiple conformations of aminoglycosides bound to *Enterococcus faecium* AAC(6′)-Ii and AAC(3) were determined using NMR spectroscopy [12, 13]. Figure 4B shows one monomer of *S. enterica* AAC(6′)-Iy and *M. tuberculosis* AAC(2′) oriented to highlight the similarities of the monomer fold and the conformation of bound CoA. The three rings of ribostamycin assume the same ring puckers in both complexes, and the deoxystreptamine and 2,6-dideoxy-2,6-diamino glucose rings are nearly perpendicular to each other in both complexes. In the AAC(6′) complex, the hydroxyl and amino substituents of the deoxystreptamine and primed ring make interactions directly or via intervening water molecules with residues on N-terminal structural elements, including β3, β4, and α2. In the AAC(2′) complex, α2 covers these strands, and ribostamycin interacts with

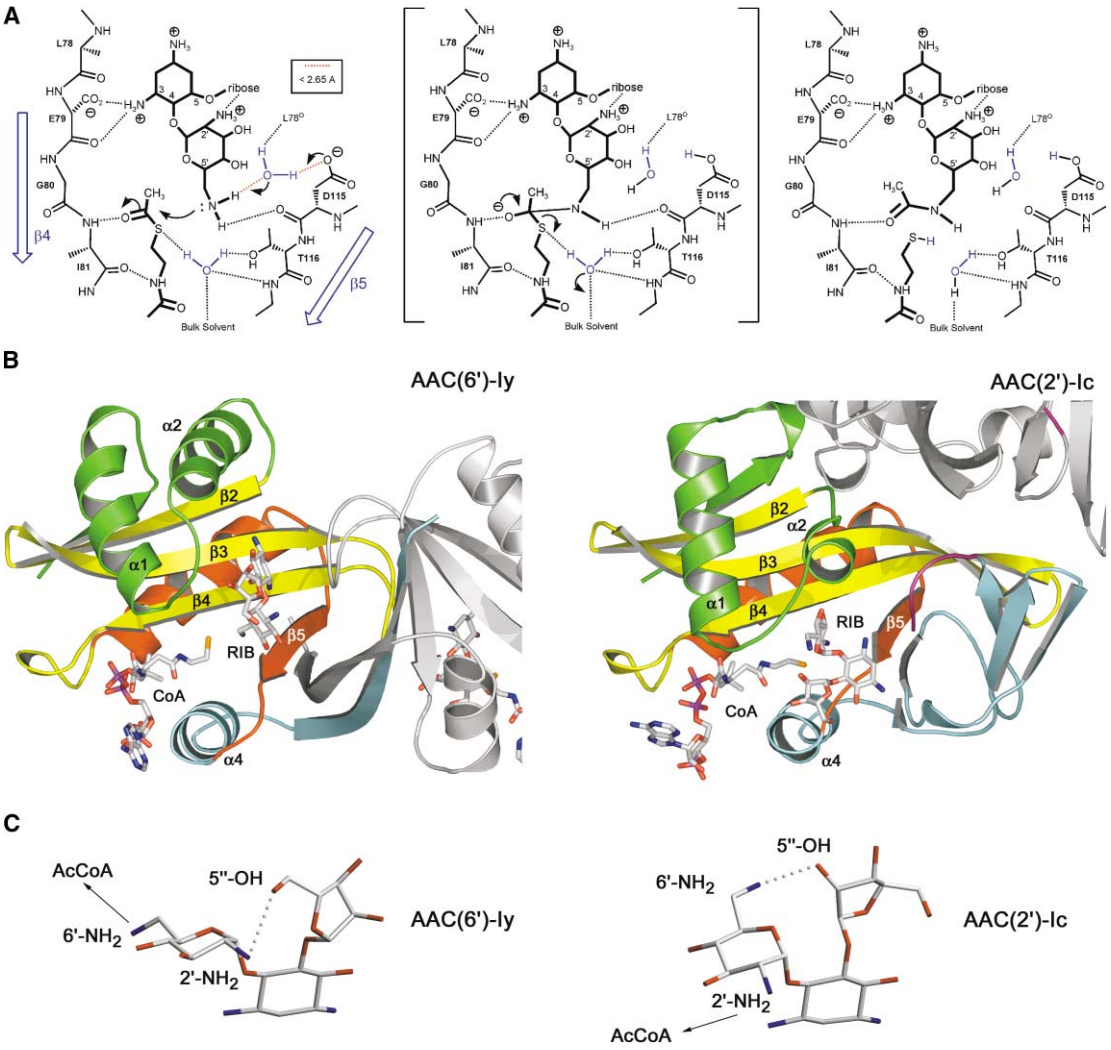

Figure 4. Comparison of AAC(6′)-Iy and AAC(2′)-Ic

(A) Proposed chemical mechanism of *S. enterica* AAC(6′)-Iy aminoglycoside N-acetyltransferase.

(B) Aligned views of a single active site of the AAC(6′)-Iy-CoA-ribostamycin and the *M. tuberculosis* AAC(2′)-CoA-ribostamycin complexes, respectively. The monomers are aligned to maximize the overlap of the monomer and bound CoA molecules. Opposing monomers of the dimer are colored in gray.

(C) Conformations of bound ribostamycin in the *S. enterica* AAC(6′)-Iy-CoA-ribostamycin and the *M. tuberculosis* AAC(2′)-CoA-ribostamycin complexes, respectively. The central, deoxystreptamine ring was used to align the two molecules.

residues on C-terminal structural elements, including β5, β9, and α4, and the C-terminal carboxylate of W181 of the same monomer. In the AAC(6′) complex, the 2′-amino group of ribostamycin makes an interaction with the 5″-hydroxyl group of the ribose ring (Figure 4C), and this interaction is stabilized by an interaction between the 2″-hydroxyl group and the imidazole ring of H25, located on the short loop connecting α1 and α2. This intramolecular interaction orients the 6′-amino group toward acetylCoA. In contrast, a minor rotation about the pseudoglycosidic linkage of ribostamycin in the AAC(2′) complex moves the 6′-amino group toward the ribose ring. The ribose ring is rotated almost 180° relative to its position in the AAC(6′) complex, and the 2″-hydroxyl now makes an intramolecular hydrogen bond with the 6′-amino group, thus orienting the 2′-amino group toward acetylCoA. These remarkably subtle differences define the regioselectivity of the two reactions catalyzed by these structurally similar enzymes.

Dimer Interface and Protein Acetylation

The monomer fold of AAC(6′)-Iy is similar to many of the previously determined aminoglycoside *N*-acetyltransferases and other GNAT superfamily members. However, the unique subunit interactions that generate the active dimer create a structure that is most structurally similar to the tetrameric, 163 amino acid *S. cerevisiae* Hpa2 histone acetyltransferase [14], with a root-mean-square deviation for 134 of the 145 amino acids of AAC(6′)-Iy of 1.42 Å, despite sharing only 19.6% primary sequence identity. Like AAC(6′)-Iy, the Hpa2 dimer is generated by similar subunit interactions, including the β6 strand exchange noted above. A superposition of the AAC(6′)-Iy and Hpa2 dimers is shown in Figure 5A.

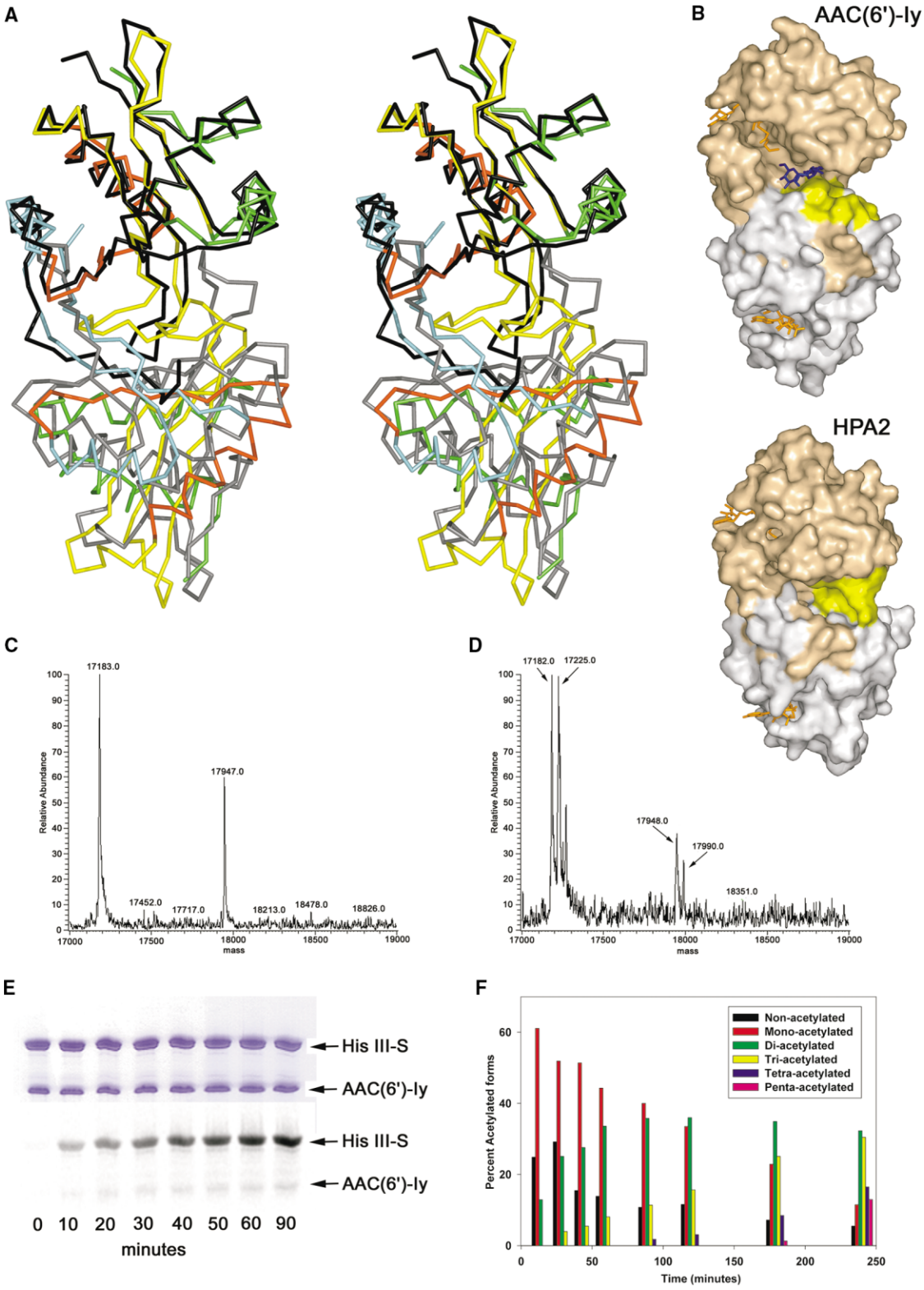

Figure 5. Comparison of AAC(6′)-Iy and HPA2

(A) Overlay of AAC(6′)-Iy dimer and the yeast Hpa2 histone acetyltransferase. AAC(6′)-Iy is colored as in Figure 2A, while the two monomers of Hpa2 are colored in black (top) and gray (bottom).

(B) Space-filling models of AAC(6′)-Iy and Hpa2. Bound CoA is colored in orange, and ribostamycin is colored in blue. The loop region connecting β3 and β4 is highlighted in yellow in both models.

(C and D) MALDI-TOF mass spectrum of AAC(6′)-Iy-His_6 before (C) and after (D) overnight incubation with acetyl-CoA.

(E) Top, Coomassie-stained SDS-PAGE of the time course of acetylation of calf thymus histone III-S by AAC(6′)-Iy. Bottom, autoradiogram of gel shown above.

(F) Time course of acetylation of human histone H3 peptide (100 μM) by AAC(6′)-Iy (0.1 mg/ml) and acetyl-CoA (200 μM). MALDI-TOF mass spectrometry of the reaction mixtures was used to qualitatively (peak height of each species/total peak height of all species) define the acetylation state of the peptide.

The major difference occurs at the dimer interface, specifically in the loop connecting β3 and β4. A structure-based sequence alignment reveals a three-residue deletion in Hpa2, resulting in a shorter connecting loop that truncates the channel at the dimer interface leading away from CoA (shown in yellow in Figure 5B).

The structural similarity of the bacterial AAC(6′)-Iy with the yeast Hpa2 histone acetyltransferase, the similar position of binding of aminoglycoside substrates and peptides, and the negatively charged surface of the dimer interface led us to explore the possibility that AAC(6′)-Iy-His_6 (C-terminal His_6 affinity tag) could acetylate cationic proteins or peptides. Incubation of the enzyme with [acetyl-^{14}C]acetyl-CoA resulted in the time-dependent acetylation of the enzyme (data not shown). In order to confirm this autoacetylation, we performed mass spectrometry (MS) on AAC(6′)-Iy-His_6 before and 16 hr after the addition of acetyl-CoA. The molecular mass of the carboxy-terminal His_6-tagged enzyme was calculated to be 17,184.3, and the major peak we observed exhibited a mass of 17,183 prior to incubation with acetyl-CoA, indicative of the nonacetylated full-length protein (Figure 5C). An additional peak was observed at a molecular mass of 17,947, a mass shift of 764 Da, corresponding to the AAC(6′)-Iy-His_6-CoA complex (predicted mass + CoA = 17,951). This is a noncovalent but extremely tightly bound complex that remains partially intact in the mass spectrometer, supporting our kinetic data concerning the rate-limiting nature of CoA release [6]. Overnight incubation of the enzyme with acetyl-CoA resulted in the appearance of a major mass-shifted peak at 17,225, corresponding to the mono-acetylated enzyme (expected: monoacetylated; 17,226 Da, Figure 5D) and a similar shift in the enzyme-CoA complex. While it is likely that acetylation occurs on the native α-amino-N-terminus of the C terminally His_6-tagged construct based on data presented below, neither the locus nor the physiological significance of the acetylation is known.

In order to most easily identify the position of acetylation, we used the N terminally extended AAC(6′)-Iy, whose structure we determined and examined the acetylation reaction with [acetyl-^{14}C]acetyl-CoA. This also became acetylated, as evidenced by SDS-PAGE followed by autoradiography (data not shown). Autoacetylation using unlabeled acetyl-CoA followed by thrombin cleavage allowed us to determine the mass of the protein and N-terminal peptide. A single peak corresponding to the predicted mass of the cleaved, nonacetylated enzyme was observed after thrombin cleavage either in the absence or presence of acetyl-CoA (predicted, 16,643.8; observed, 16,642), suggesting that acetylation occurs on the N-terminal peptide. Incubation with acetyl-CoA followed by thrombin cleavage yielded two peptide peaks corresponding to the predicted mass of the des-methionine acetylated peptide (predicted, 1810; observed, 1811) and a second peak corresponding to a des-methionine, di-acetylated peptide (predicted, 1852, observed, 1854). Using tandem mass spectrometry, we identified the N-terminal glycine residue as the site of the first, stoichiometric acetylation. This requires that the enzyme catalyze its own α-*N* acetylation after post-translational enzymatic deformylation and removal of the initiator methionine. The second acetylation, which represents ~15% of the total peptide, was unambiguously assigned as occurring on the second histidine in the His_6 sequence (H5). The α-*N*-terminal acetylation of the N terminally His_6-tagged construct (Figure 5E) likely occurs intermolecularly and is not likely to be physiologically significant.

The *S. enterica N*-acetyltransferase is also an efficient histone acetyltransferase. As shown in Figure 5E, incubation of calf thymus histone III-S preparations with AAC(6′)-Iy-His_6 and [acetyl-^{14}C]-acetyl-CoA led to very rapid histone acetylation, which can be compared to the very slow relative rate of AAC(6′)-Iy autoacetylation. In order to determine whether histone acetylation by the bacterial N-acetyltransferase is stoichiometric and regioselective, we determined the ability of AAC(6′)-Iy to acetylate the 21 amino acid human histone H3 N-terminal peptide (ARTK_4QTARK_9STGGK_{14}A-PRK_{18}QLC). This peptide is rapidly monoacetylated (~60% in 15 min) and more slowly diacetylated, and after long incubation times, tri-, tetra-, and penta-acetylated forms of the peptide are observed (Figure 5F). Base treatment prior to MS argues that acetylation is occurring exclusively on amino groups. This kinetic discrimination is most likely the result of regioselective acetylation, although we have no information presently on the order in which the 4 ε-amino groups of lysine or the α-N terminus are acetylated. Two other bacterial GNAT superfamily members, the *E. faecium* AAC(6′)-Ii [9] and tabtoxin resistance protein [15], have been shown to be capable of acetylating histones, but no analysis of either the stoichiometry or regioselectivity of the acetylation was reported.

An unanswered question of the present study remains the identification of the physiological function of this chromosomally encoded GNAT. The genomic environment of the gene, directly behind a long operon containing both sugar transporter homologs and putative sugar metabolizing enzymes [5], may suggest a function in sugar metabolism. However, the enzyme is incapable of O-acetylation, suggesting that it could only function in aminosugar metabolism. While documented to catalyze aminoglycoside 6′-*N*-acetylation [6], it is also unlikely that this represents a true physiological role. Our demonstration that the enzyme can efficiently *N*-acetylate proteins suggests a more reasonable physiological role, although the protein or peptide substrate or substrates remain unknown.

Significance

The enzymological demonstration that AAC(6′)-Iy binds aminoglycosides, proteins, and peptides and can both α-*N*-acetylate its amino terminus and regioselectively acetylate aminoglycosides and a mammalian histone peptide is remarkable. The structure that we present here of the *S. enterica* AAC(6′)-Iy has revealed a long, highly anionic channel generated at the dimer interface and leading into the active site, where both aminoglycoside antibiotics and peptides are bound. Many of the same active site residues interact with both aminoglycoside and peptide. The structure of the acetyltransferase dimer is highly similar to the

S. cerevisiae **Hpa2 histone acetyltransferase, including the β6 exchange observed at the dimer interface in both enzymes but not in other bacterial aminoglycoside *N*-acetyltransferases. Taken together, these data argue that bacterial acetyltransferases, including those identified as aminoglycoside acetyltransferases, are the evolutionary progenitors of the well-studied eukaryotic histone acetyltransferases.**

The extension of the structural and catalytic correlations between pro- and eukaryotic GNAT superfamily members, demonstrated here, to physiological functions of regulation is tempting. In bacteria, there are only three enzymes proposed to catalyze protein acetylation. These are the RimJ, RimI, and RimL α-N-acetyltransferases [16] that act on three ribosomal proteins, S5, S18, and L12, all located near the acceptor site in the bacterial ribosome. The acetylation state of L12, whose N terminally acetylated product is termed L7, is known to be correlated with growth phase, being lowest during logarithmic growth and highest in stationary phase [17]. A different protein acetylation modification has been reported for *Salmonella enterica* acetyl-CoA synthetase, where acetylation of the active site Lys609 has been shown to inactivate the enzyme [18]. Although the enzyme that catalyzes acetylation of this residue is not known, protein acetylation by *N*-acetyltransferases in bacteria, both at the N termini and at internal lysine residues, may serve important regulatory roles similar to those documented in eukaryotes.

Experimental Procedures

Protein Expression and Structure Determination

The *S. enterica* AAC(6′)-Iy was expressed in *Escherichia coli* from the pET23 vector with a directly attached C-terminal His_6 tag or, for structural studies, from the pET28a vector. Therefore, all crystals contain an N-terminal His_6 affinity tag and thrombin cleavage sequence. Three crystal forms of AAC(6′)-Iy were obtained by vapor diffusion under oil. $P3_121$ crystals grew from 4 μl drops consisting of 2 μl of protein (15 mg/ml, 20 mM triethanolamine [TEA] pH 8.0, 100 mM $(NH_4)_2SO_4$) and 2 μl of 2 M $(NH_4)_2SO_4$. Crystals were immersed in a solution of 100 mM TEA (pH 8.0), 2 M $(NH_4)_2SO_4$, and 20% glycerol prior to vitrification by immersion in liquid nitrogen. $P3_221$ crystals grew from 4 μl drops consisting of 2 μl of protein (15 mg/ml, 20 mM TEA [pH 8.0], 100 mM $(NH_4)_2SO_4$), 2 μl of 1.5 M $(NH_4)_2SO_4$, and 25 mM Bicine (pH 8.8). Crystals were immersed in a solution of 100 mM Bicine (pH 8.8), 2 M $(NH_4)_2SO_4$, and 28% xylitol prior to vitrification by immersion in liquid nitrogen. The ribostamycin complex crystal form grew from 4 μl drops consisting of 2 μl of protein (15 mg/ml, 20 mM TEA [pH 8.0], 100 mM $(NH_4)_2SO_4$, 0.6 mM CoA, 0.4 mM ribostamycin) and 2 μl of 20% polyethylene glycol 3350. Crystals were immersed in a solution of 100 mM TEA (pH 8.0), 20% polyethylene glycol 3350, 100 mM $(NH_4)_2SO_4$, 0.4 mM ribostamycin, and 20% glycerol prior to vitrification by immersion in liquid nitrogen. A three wavelength anomalous diffraction (MAD) experiment was performed with a Se-Met-substituted $P3_221$ crystal form at beamline X9A of the NSLS. The MAD data sets were processed with DENZO and SCALEPACK [19]. Se-Met positions were determined by SNB [20] and refined in SOLVE [21]. A rough initial main chain trace was built into a solvent flattened MAD map and used as a molecular replacement model to determine the position of the dimer in the $P3_121$ crystal form. Solvent flattening, histogram matching, cross-crystal 3-fold averaging, and phase extension within the program DMMULTI [22] utilizing the MAD data and the $P3_121$ crystal form yielded phases to 2.4 Å and a traceable map. The program MAID [23] was used to autofit a majority of the structure, while the remaining portions were manually built using the program O [24]. The program AMORE [25] was used to obtain the molecular replacement solution for the cross-crystal averaging and to determine the initial phases for the ribostamycin complex. All structures were refined in the program CNS [26]. A subset (5%) of the data was excluded from all steps of refinement and used only for the calculation of the R_{free} [27]. The $P3_121$ (Native 1) crystal form contains a molecular dimer in the asymmetric unit (ASU): monomer A (residues 1–145 plus 8 residues from the His_6 tag) and monomer B (residues 2–145 minus residues 22–31). The $P3_221$ (Native 2) crystal form contains a monomer per ASU: monomer A (residues 1–145 plus 7 residues from the His_6 tag). The ribostamycin complex contains a molecular dimer per ASU: monomer A (residues 1–145 plus 2 residues from the His_6 tag) and subunit B (residues 1–145). In all structures, there is one CoA and one sulfate ion bound per monomer. Ribostamycin is bound to both monomers in the ribostamycin complex. Root-mean-square deviations between various monomeric structures ranged from 0.34–0.66 $Å^2$.

Protein and Peptide Acetylation

Incubation of *S. enterica* AAC(6′)-Iy with [^{14}C-acetyl]-acetylCoA (Amersham) was performed overnight. Samples were heat denatured (100°C) in 0.1% SDS containing 1 mM β-mercaptoethanol in loading buffer containing dye for 3 min. PAGE was run on 10%–15% gradient PhastGels using the PhastSystem (Pharmacia). Calf thymus histone preparation III-S (3 mg/ml, Sigma) was incubated with an equivalent concentration of *S. enterica* AAC(6′)-Iy and [^{14}C-acetyl]-acetylCoA for times from 0–90 min, followed by rapid heat denaturation as described above. After SDS-PAGE as above, gels were stained with Coomassie blue and destained, air dried, covered with plastic, and exposed for 24 hr in a ImagePlate cassette. Radioactivity was detected using a Storm 28 Phosphoimager system (Amersham-Pharmacia Biotech.) and quantitated using the ImageQuant 5.2 software provided by the manufacturer. Human histone H3 peptide containing a C-terminal cysteine residue (100 μM,Upstate Biotechnology) was incubated in 25 mM NH_4HCO_3 and 200 μM acetyl-CoA. The reaction was initiated by the addition of AAC(6′)-Iy (final concentration 40 μg/ml), and at the indicated time intervals reactions were quick frozen and lyophilized. The samples were taken up in 0.1% TFA and mixed 1:1 with a saturated solution of α-cyano-4-hydroxycinnamic acid in 50% aqueous acetonitrile containing 0.1% TFA. Matrix-assisted laser desorption ionization time-of-flight (MALDI-TOF) mass spectrometry was performed using an Applied Biosystems Voyager-DE mass spectrometer.

Acknowledgments

This work was supported by NIH grant AI33696.

Received: December 18, 2003
Revised: January 27, 2004
Accepted: January 30, 2004
Published: April 16, 2004

References

1. Wright, G.D., Berghuis, A.M., and Mobashery, S. (1998). Aminoglycoside antibiotics. Structures, functions, and resistance. Adv. Exp. Med. Biol. *456*, 27–69.
2. Honore, N., Marchal, G., and Cole, S.T. (1995). Novel mutation in 16S rRNA associated with streptomycin dependence in *Mycobacterium tuberculosis*. Antimicrob. Agents Chemother. *39*, 769–770.
3. Wright, G.D. (1999). Aminoglycoside-modifying enzymes. Curr. Opin. Microbiol. *2*, 499–503.
4. The Aminoglycoside Resistance Study Groups. (1995). The most frequently occurring aminoglycoside resistance mechanisms: combined results of surveys in eight regions of the world. J. Chemother. *7* (*Suppl. 2*), 17–30.
5. Magnet, S., Courvalin, P., and Lambert, T. (1999). Activation of the cryptic aac(6′)-Iy aminoglycoside resistance gene of Salmonella by a chromosomal deletion generating a transcriptional fusion. J. Bacteriol. *181*, 6650–6655.
6. Magnet, S., Lambert, T., Courvalin, P., and Blanchard, J.S.

(2001). Kinetic and mutagenic characterization of the chromosomally encoded *Salmonella enterica* AAC(6′)-Iy aminoglycoside N-acetyltransferase. Biochemistry *40*, 3700–3709.
7. Hegde, S.S., Dam, T.K., Brewer, C.F., and Blanchard, J.S. (2002). Thermodynamics of aminoglycoside and acyl-coenzyme A binding to the *Salmonella enterica* AAC(6′)-Iy aminoglycoside N-acetyltransferase. Biochemistry *41*, 7519–7527.
8. Wolf, E., Vassilev, A., Makino, Y., Sali, A., Nakatani, Y., and Burley, S.K. (1998). Crystal structure of a GCN5-related N-acetyltransferase: *Serratia marcescens* aminoglycoside 3-N-acetyltransferase. Cell *94*, 439–449.
9. Wybenga-Groot, L.E., Draker, K., Wright, G.D., and Berghuis, A.M. (1999). Crystal structure of an aminoglycoside 6′-N-acetyltransferase: defining the GCN5-related N-acetyltransferase superfamily fold. Struct. Fold. Des. *7*, 497–507.
10. Dyda, F., Klein, D.C., and Hickman, A.B. (2000). GCN5-related N-acetyltransferases: a structural overview. Annu. Rev. Biophys. Biomol. Struct. *29*, 81–103.
11. Vetting, M.W., Hegde, S.S., Javid-Majd, F., Blanchard, J.S., and Roderick, S.L. (2002). Aminoglycoside 2′-N-acetyltransferase from *Mycobacterium tuberculosis* in complex with coenzyme A and aminoglycoside substrates. Nat. Struct. Biol. *9*, 653–658.
12. DiGiammarino, E.L., Draker, K.A., Wright, G.D., and Serpersu, E.H. (1998). Solution studies of isepamicin and conformational comparisons between isepamicin and butirosin A when bound to an aminoglycoside 6′-N-acetyltransferase determined by NMR spectroscopy. Biochemistry *37*, 3638–3644.
13. Owston, M.A., and Serpersu, E.H. (2002). Cloning, overexpression, and purification of aminoglycoside antibiotic 3-acetyltransferase-IIIb: conformational studies with bound substrates. Biochemistry *41*, 10764–10770.
14. Angus-Hill, M.L., Dutnall, R.N., Tafrov, S.T., Sternglanz, R., and Ramakrishnan, V. (1999). Crystal structure of the histone acetyltransferase Hpa2: A tetrameric member of the Gcn5-related N-acetyltransferase superfamily. J. Mol. Biol. *294*, 1311–1325.
15. He, H., Ding, Y., Bartlam, M., Sun, F., Le, Y., Qin, X., Tang, H., Zhang, R., Joachimiak, A., Liu, J., et al. (2003). Crystal structure of tabtoxin resistance protein complexed with acetyl coenzyme A reveals the mechanism for beta-lactam acetylation. J. Mol. Biol. *325*, 1019–1030.
16. Bradshaw, R.A., Brickey, W.W., and Walker, K.W. (1998). N-terminal processing: the methionine aminopeptidase and N alpha-acetyl transferase families. Trends Biochem. Sci. *23*, 263–267.
17. Ramagopal, S., and Subramanian, A.R. (1974). Alteration in the acetylation level of ribosomal protein L12 during growth cycle of Escherichia coli. Proc. Natl. Acad. Sci. USA *71*, 2136–2140.
18. Starai, V.J., Celic, I., Cole, R.N., Boeke, J.D., and Escalante-Semerena, J.C. (2002). Sir2-dependent activation of acetyl-CoA synthetase by deacetylation of active lysine. Science *298*, 2390–2392.
19. Otwinski, Z. (1993). In Proceedings of the CCP4 Study Weekend, L. Sawer, ed. (Warrington, United Kingdom: Daresbury Laboratory), pp 55–62.
20. Hauptman, H.A. (1997). Shake-and-Bake: An algorithm for automatic solution ab initio of crystal structures. Methods Enzymol. *277*, 3–13.
21. Terwilliger, T.C., and Berendzen, J. (1999). Automated MAD and MIR structure solution. Acta Crystallogr. D Biol. Crystallogr. *55*, 849–861.
22. CCP4 (Collaborative Computational Project Number 4) (1994). The CCP4 suite: programs for protein crystallography. Acta Crystallogr. D Biol. Crystallogr *50*, 760–763.
23. Levitt, D.G. (2001). A new software routine that automates the fitting of protein X-ray crystallographic electron-density maps. Acta Crystallogr. D Biol. Crystallogr. *57*, 1013–1019.
24. Jones, T.A., Zou, J.Y., Cowan, S.W., and Kjeldgard, M. (1991). Improved methods for finding protein models in electron density maps and location of error in these models. Acta Crystallogr. A *47*, 110–119.
25. Navaza, J. (2001). Implementation of molecular replacement in AMoRe. Acta Crystallogr. D Biol. Crystallogr. *57*, 1367–1372.
26. Brunger, A.T. (1998). Crystallographry & NMR system: A new software suite for macromolecular structure determination. Acta Crystallogr. D Biol. Crystallogr. *54*, 905–921.
27. Brunger, A.T. (1992). Free R value: A novel statistical quantity for assessing the accuracy of crystal structures. Acta Crystallogr. D Biol. Crystallogr. *49*, 24–46.
28. Nicholls, A., Bharadwaj, R., and Honig, B. (1993). GRASP: graphical representation and analysis of surface proteins. Biophys. J. *64*, A166.

Accession Numbers

The coordinates and structure factors of the two AAC(6′)-Iy binary complexes (accession codes 1S5K and 1S60) and the AAC(6′)-Iy ternary complex (accession code 1S3Z) have been deposited in the Protein Data Bank.